



Cite this: *Dalton Trans.*, 2025, **54**, 5446

New insights into bioactive Ga(III) hydroxyquinolinate complexes from UV-vis, fluorescence and multinuclear high-field NMR studies†‡

Vanessa V. Gaensicke,^a Stephanie Bachmann,^b Luca Craciunescu,^c Andrew W. Prentice,^c Martin J. Paterson,^c Dinu Iuga,^b Peter J. Sadler^{ID, *a} and Rafael Cavalieri Marchi^{ID, *a,d}

There is current interest in the anticancer and antimicrobial activities of Ga(III) tris-hydroxyquinolinate complexes, and hence their solution and solid-state chemistry. Here, we have studied the formation, stability and structure of a novel tris-5,7-dibromo-8-hydroxyquinolinate Ga(III) complex $[\text{Ga}(\text{Br}_2\text{-HQ})_3]$. Reactions of 5,7-dibromo-8-hydroxyquinoline with $\text{Ga}(\text{NO}_3)_3$ in DMSO were followed using electronic absorption and emission spectroscopy, and revealed the slow but concerted coordination of three chelated ligands, with ligand deprotonation being the apparent rate-limiting step, facilitated by basic Ga(III) hydroxido species. The emissive excited state of $[\text{Ga}(\text{Br}_2\text{-HQ})_3]$ in DMSO had a short half-life of 1.2 ns, and the fluorescence (550 nm, $\lambda_{\text{ex}} = 400$ nm) was characterized by TDDFT calculations as arising from a ligand-centred singlet S1 state. We compared the structures of $[\text{Ga}(\text{Br}_2\text{-HQ})_3]$ and the clinical tris-hydroxyquinolinate complex $[\text{Ga}(\text{HQ})_3]$ using high-field magic-angle-spinning solid-state 1D and 2D 850 MHz and 1 GHz ^1H , ^{13}C and ^{71}Ga NMR spectroscopy. The similarity of their coordination spheres was confirmed by their ^{71}Ga chemical shifts of 101 and 98 ppm, respectively, and quadrupolar coupling constants of 9.265 MHz and 9.282 MHz. ^1H - ^1H 2D NOESY experiments revealed second coordination sphere interactions between an acetic acid solvent molecule and the bound hydroxyquinolinate ligands of $[\text{Ga}(\text{HQ})_3] \cdot 0.5\text{CH}_3\text{CO}_2\text{H}$. This finding suggests that carboxylic acids could play a role in modifying the formulation properties of this drug for clinical use.

Received 13th January 2025,
Accepted 15th February 2025

DOI: 10.1039/d5dt00087d

rsc.li/dalton

1. Introduction

Gallium(III) has gained increasing attention due to its therapeutic applications with low toxicity. Several Ga(III) complexes are currently either in clinical use or being explored as anti-cancer agents.^{1,2}

The first clinical use of Ga(III) in 1970 involved the radioactive isotope ^{67}Ga as an imaging agent. Now both ^{67}Ga and ^{68}Ga (single-photon emission computed tomography and positron

emission tomography, respectively)³ are used for, *e.g.*, soft tissue and bone tumours, along with inflammatory abscesses.⁴ In 2003, a citrate-buffered formulation of Ga(III) nitrate was approved by the US Food and Drug Administration (FDA) as Ganite® for the treatment of malignancy-associated hypercalcaemia,^{5,6} non-Hodgkin's lymphoma⁵ and bladder cancer.⁷ Several other Ga(III) complexes and formulations are undergoing phase I and II clinical trials for cancer treatment.^{2,8}

Ga(III) complexes are also known to possess good antimicrobial activity. Recently, an extensive screening of compounds by the community of open antimicrobial drug discovery (CO-ADD) has shown that the hit-rate for metal complexes (906 complexes screened; 27% active) was higher than for organic compounds (almost 300 000; 2% active) against Gram-negative and Gram-positive bacteria.⁹ Notably, Ga(III) complexes were highly active, although only a few were screened.^{9,10}

The mechanism of biological action of Ga(III) complexes is believed to involve interference in natural Fe(III) biochemistry. Both ions have similar radii and coordination chemistry, however unlike Fe(III), Ga(III) is not redox-active. For instance, gallium-sub-

^aDepartment of Chemistry, University of Warwick, Coventry, CV4 7AL, UK.

E-mail: P.J.Sadler@warwick.ac.uk, Rafael.Marchi@warwick.ac.uk

^bDepartment of Physics, University of Warwick, Coventry, CV4 7AL, UK

^cSchool of Engineering and Physical, Heriot-Watt University, Edinburgh, EH14 4AS, UK

^dInstitute of Advanced Studies (IAS), University of Warwick, Coventry, CV4 7AL, UK

†This paper is dedicated to Rudi van Eldik on the occasion of his 80th birthday and in celebration of his excellent contributions to inorganic chemistry over many years.

‡ Electronic supplementary information (ESI) available. See DOI: <https://doi.org/10.1039/d5dt00087d>



stituted enzymes and proteins affect the survival of microorganisms since they cannot exert the functions of their iron-dependent counterparts, leading to metabolic disruption.^{1,11} Ga(III) can contribute to deregulation of cellular iron homeostasis.¹²

Hydroxyquinolines act as bidentate ligands through coordination of the deprotonated hydroxyl oxygen and the ring nitrogen (Fig. 1). These ligands can inhibit several enzymes including topoisomerase and haspin kinase.^{13,14} Use of hydroxyquinolines as ligands for Ga(III) can result in a scaffold suitable for drug development. The tris-chelated 8-hydroxyquinoline (HQH) as [Ga(HQ)₃] is currently in phase II clinical trials as the oral gallium compound KP46 for treatment of breast, lung, and prostate cancer and bone metastases.¹⁵ Interestingly, *in vivo* trace studies with radioactive (⁶⁷Ga and ⁶⁸Ga) KP46, suggest that oral administration can lead to dissociation of the complex in the gut.¹⁵

The aqueous solution chemistry of Ga(III) is complicated by hydrolysis and formation of hydroxido/oxido monomers and oligomers, as is the case for Fe(III) and widely studied Al(III).^{16–20} Equilibria between hydrolysed species can be both thermodynamically and kinetically driven. For aqua Ga(III) complexes, pK_a values range from 2.6 (formation of Ga(OH)²⁺) to 6.3 (formation of Ga(OH)₄[−]).^{21–23} Hence, hydrolysed Ga(III) species are likely to play a role in the biological chemistry of gallium.

In this work we have studied binding of the 8-hydroxyquinoline derivative 5,7-dibromo-8-hydroxyquinoline (Br₂-HQH) to Ga(III). The ligand was chosen to provide the possibility of tracking both Ga(III) and the ligand in biological cells using elemental X-ray imaging, as we have done for an organosmium anticancer complex with a brominated chelated ligand.²⁴ This method allows identification of dissociation of a bound Br-labelled ligand from a metal in cells.

We studied the binding of Br₂-HQH to Ga(NO₃)₃ in a variety of organic and aqueous solvents using UV-visible, fluorescence and NMR spectroscopy. The luminescence lifetime of the product was determined, and emissive state was characterised by DFT calculations. Under certain conditions it was possible to isolate [Ga(Br₂-HQ)₃] which was characterised by multinuclear NMR spectroscopy, including ⁷¹Ga and comparison with the clinical drug [Ga(HQ)₃], Fig. 1. Although ⁷¹Ga is a quadrupole nucleus (39.89% natural abundance, $I = 3/2$)²⁵ giving relatively broad resonances in non-symmetrical environments, its resonances are sharper at high fields such as 20 T and 23.5 T since the magic angle spinning (MAS) quadrupolar broadening of the central transition is inversely proportional to the external magnetic field.

2. Methods and materials

2.1. Materials

Ga(NO₃)₃·3H₂O (99.9%) was purchased from abcr UK Ltd and 5,7-dibromo-8-hydroxyquinoline from Aldrich (98%). All other solvents and reagents were purchased from Sigma-Aldrich and used without further purification. 72% *v/v* nitric acid (HNO₃) was freshly distilled and diluted with milliQ water. The gallium standard for ICP was TraceCERT® 1 g L^{−1} Ga in nitric acid.

2.2. Synthesis of [Ga(Br₂-HQ)₃]

5,7-Dibromo-8-hydroxyquinoline (2.85 g, 9.41 mmol) was dissolved in DMF (10 mL) and Ga(NO₃)₃·3H₂O (0.962 g, 3.76 mmol) in 3 mL Milli-Q water. Both solutions were poured into warm acetonitrile (100 mL, 318 K) and a yellow precipitate formed. The precipitate was isolated by filtration, washed with MeCN (2 × 10 mL), dried under vacuum for 6 h and stored at 277 K overnight. The solid was dried at 310 K for 12 h giving a fine, yellow powder (2.25 g, 74% yield). Elemental analysis % CHNGa: found 33.01, 1.25, 4.52, 6.98; calculated 33.24, 1.24, 4.32, 7.08. ESI MS: [M + Na]⁺ observed *m/z* = 997.5031, calculated *m/z* = 997.5072.

2.3. Synthesis of [Ga(HQ)₃]

The synthetic protocol was based on a literature report.²⁶ Briefly, 8-hydroxyquinoline (1.37 g, 9.41 mmol) was dissolved in aqueous 10% acetic acid followed by the addition of Ga(NO₃)₃·3H₂O (0.962 g, 3.76 mmol). A yellow precipitate formed, and the reaction was heated at 353 K for 1 h. The precipitate was isolated and washed with hot water (0.5 L), cold water (0.5 L) and diethylether (50 mL). The solid was dried under vacuum for 24 h to give a fine yellow powder (1.91 g, 81%). ¹H-NMR: (DMSO-*d*₆ 500 MHz) δ : 8.72 (d, 2H), 8.58 (m, 3H), 7.66 (d, 2H), 7.51 (m, 5H), 7.18 (d, 3H), 6.88 (m, 3H). The peaks in the aromatic region are similar to those previously reported;¹⁵ assignments are complicated by the presence of isomers. Additional signals were observed at 1.73 and 11.8 ppm which are assignable to the methyl and hydroxyl protons, respectively, of CH₃CO₂H (¹H-¹H NMR exchange cross peak for -COOH/H₂O at 11.98/3.33), which integrated as 0.5 mol per mol complex, Fig. S1.‡ The solid state ¹H-NMR spectrum confirmed the presence of CH₃CO₂H (section 3.3).

2.4. ¹H-¹H NOESY

The ¹H 2D NOESY NMR spectrum of [Ga(HQ)₃]·0.5CH₃CO₂H in DMSO-*d*₆ was acquired at 298 K on a Bruker AVIII-500 spectrometer at 500.13 MHz in a 5 mm NMR tube. The spec-

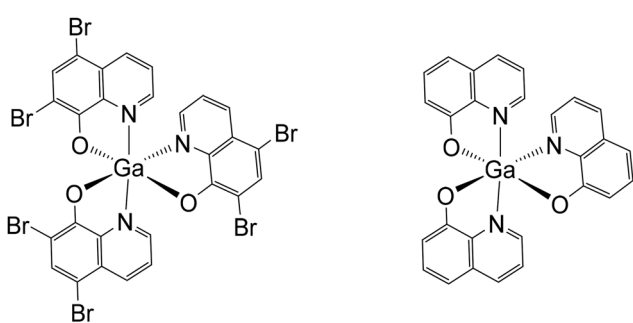


Fig. 1 Chemical structures of *mer*-[Ga(Br₂-HQ)₃] and *mer*-[Ga(HQ)₃] studied in this work.

trum was recorded using a standard pulse sequence (2D homonuclear correlation *via* dipolar coupling with gradient pulses in the mixing time). Typically, data were acquired with 16 accumulations and 2048×256 sampling data points with a NOESY mixing time of 0.6 s. Data processing was carried out using XWIN-NMR version 3.2 (Bruker U.K. Ltd).

2.5. Infrared (IR) spectroscopy

Powdered sample was placed on the surface of a Bruker Alpha II Compact FT-IR spectrometer at 298 K and IR spectra were recorded from 4000 to 450 cm^{-1} with OPUS software using 64 scans.

2.6. UV-vis spectroscopy

UV-vis spectra were recorded on an Agilent Cary 300 UV-vis spectrophotometer with 1-cm path-length quartz cuvettes at 298 K. For the *titration experiments* 44 mM solutions of $\text{Br}_2\text{-HQH}$ and $\text{Ga}(\text{NO}_3)_3 \cdot 3\text{H}_2\text{O}$ were prepared in DMF and Milli-Q water, respectively. An aliquot (10.3 μL) of $\text{Br}_2\text{-HQH}$ in DMF was diluted with DMSO to 3.0 mL in the cuvette giving a final concentration of 0.15 mM. This procedure provided the necessary solubility of $\text{Br}_2\text{-HQH}$ to allow reactions to be carried out in DMSO (containing 0.4% v/v DMF). For the titration, aliquots (0.6 μL) of $\text{Ga}(\text{iii})$ stock solution were added to the cuvette containing the ligand with mixing using a magnetic stirrer, and the spectrum was recorded after each addition. A total of 16 additions were made, giving a final 1 : 1 mol ratio of $\text{Br}_2\text{-HQH} : \text{Ga}(\text{iii})$ (0.15 mM).

A second titration was carried out with deprotonated ligand ($\text{Br}_2\text{-HQ}$) prepared by adding an equimolar concentration of NaOH to $\text{Br}_2\text{-HQH}$ in DMSO with 0.4% DMF solution, and repeating the titration adding $\text{Ga}(\text{iii})$ to the $\text{Br}_2\text{-HQ}$ solution.

To investigate the *time dependence of complex formation*, different $\text{Ga}(\text{iii})$ aliquots (3.4, 6.8, 10.2 μL) from the 44 mM stock solution were added to 3.0 mL of 0.15 mM solution of $\text{Br}_2\text{-HQH}$ in DMSO with 0.4% DMF (v/v) solution in a cuvette. The final mol ratios of $\text{Br}_2\text{-HQH} : \text{Ga}(\text{iii})$ were 1 : 0.33, 1 : 0.67, 1 : 1. The UV-vis spectrum of each solution was recorded every 3 min at 298 K for a total of *ca.* 2 h.

In each case, the plot of absorbance at 400 nm *vs.* time gave a reasonable fit to 1st-order kinetics, eqn (1):

$$\ln \left(\frac{A_f - A_t}{A_f - A_0} \right) = -kt \quad (1)$$

where A_f is the absorbance at equilibrium, A_t the absorbance at time t , and A_0 the initial absorbance.

In order to determine the influence of ligand deprotonation on the rate of complex formation, we repeated the slowest of these reactions (1 $\text{Br}_2\text{-HQH} : 0.33\text{ Ga}(\text{iii})$) but now using deprotonated ligand ($\text{Br}_2\text{-HQ}$) prepared as above and adding 0.33 mol equiv. $\text{Ga}(\text{iii})$. The spectrum of the solution was recorded every 3 minutes at 298 K for a total of 2 h.

2.7. Fluorescence

Fluorescence spectra were collected on an Agilent Cary Eclipse fluorescence spectrometer using a 1-cm path-length custom

long-neck quartz cuvette at ambient temperature (298 K). For the *titration experiments* similar solutions were prepared as described above in section 2.5, *i.e.*, containing 0.15 mM $\text{Br}_2\text{-HQH}$ and increasing concentrations of $\text{Ga}(\text{NO}_3)_3 \cdot 3\text{H}_2\text{O}$, giving a final 1 : 1 mol ratio of $\text{Br}_2\text{-HQH} : \text{Ga}(\text{iii})$ (0.15 mM). The emission was recorded in the region between 450 nm to 750 nm with $\lambda_{\text{ex}} = 400\text{ nm}$.

2.8. Solid state NMR

^{13}C CP solid-state NMR experiments were carried out using a 4 mm HX probe and magic angle spinning (MAS) up to 12 kHz on a Bruker Avance Neo spectrometer with a ^1H Lamor frequency of 850 MHz (20 T). The optimization of the cross-polarization condition was done with L-alanine using a ^1H 90° pulse of 3 μs . ^{13}C CP MAS spectra of $[\text{Ga}(\text{HQ})_3]$ were recorded at 10 kHz, 11 kHz and 12 kHz spinning rates with 1136, 1272 and 128 scans, respectively, an interscan delay of 3 s and a contact time of 1 ms at 20 T. ^{13}C CP MAS NMR spectra of $[\text{Ga}(\text{Br}_2\text{-HQ})_3]$ were recorded under the same conditions with 935, 1024 and 160 scans, respectively. ^{13}C chemical shifts were referenced to the carbonyl carbon of L-alanine at $\delta^{(13)\text{C}} = 177.8\text{ ppm}$ in respect to tetramethylsilane (TMS) corresponding to the methylene carbon of adamantane at $\delta^{(13)\text{C}} = 38.48\text{ ppm}$.²⁷ ^1H solid state NMR one pulse experiments were carried out at 23.5 T (^1H lamor frequency of 1 GHz) and a spinning rate of 60 kHz with 4 scans and an interscan delay of 1 s. ^1H - ^1H NOESY experiments for the complexes were conducted with a 1.3 mm triple-resonance HXY probe operating in double-resonance mode at a ^1H Lamor frequency of 850 MHz with 16 scans and 128 increments with two different mixing times of 5 and 219 ms and referenced using the dipeptide $\beta\text{-AspAla}$.²⁸ ^{71}Ga experiments with double frequency sweep (DFS)²⁹ (145 to 1000 Hz sweep frequency, with 1 ms sweep duration) enhancement followed by a 90° pulse with a pulse length of 1.6250 μs were carried out with a 1.3 mm triple-resonance HXY probe operating in double-resonance mode at a magnetic field strength of 20 T or using wideband, uniform rate, smooth truncation (WURST)³⁰ shaped pulse (sweep width of 40 kHz, pulse length 1 ms) followed by a 90° pulse with a pulse length of 1 μs carried out with a 1.3 mm double-resonance HX probe at 23.5 T, respectively, with an interscan delay of 0.1 s and up to 20480 scans. ^{71}Ga resonances were referenced to 1 M $\text{Ga}(\text{NO}_3)_3$ in D_2O . Fitting of the ^{71}Ga signals was carried out with the sola module of Bruker software TopSpin 4.4.0 using one site. All measurements were carried out at 298 K. For all measurements, ZrO_2 rotors were used.

2.9. Fluorescence lifetime

Fluorescence-lifetime measurements were performed using a HORIBA Jobin Yvon Fluorolog modular spectrofluorometer. A 1 μM solution of the synthesised $[\text{Ga}(\text{Br}_2\text{-HQ})_3]$ complex in DMSO was used in a quartz fluorescence cuvette (3 mL) at ambient temperature with excitation at 405 nm and detection at 550 nm. Decay of the emission was fitted to a monoexponential decay function in Origin which included a convolution for the instrument response (0.87 ns).



2.9. Photostability

UV-vis spectra were recorded on an Agilent Cary 300 UV-vis spectrophotometer with 1-cm path-length quartz cuvettes at 298 K. A 0.05 mM solution of $[\text{Ga}(\text{Br}_2\text{-HQ})_3]$ was prepared in DMSO and 3.0 mL was pipetted into the cuvette. The sample was irradiated with blue light LED (450 nm) every 30 s for 15 min.

2.10. Inductively coupled plasma-optical emission spectroscopy (ICP-OES)

An Agilent 5800 ICP-OES spectrometer was used with gallium emission detected at 417.204 nm. Concentration standards for gallium were prepared in the range 0–1000 ppb from 10 000 ppm certified reference material in 3.6% v/v nitric acid. The correlation coefficient for the linear curve was 0.9998. Solutions of $[\text{Ga}(\text{Br}_2\text{-HQ})_3]$ in 3.6% v/v HNO_3 were analysed.

2.11. Computational methods

DFT calculations with different functionals (B3LYP, CAM-B3LYP, ω B97X-D3, RSX-QIDH and SCS- ω PBEPP86) were carried out in the Orca 5.0.3 program package.^{31–33} ADC(2)^{34–36} computations were run with the MRCC program package.^{37,38} All calculations made use of the def2-TZVP basis set for Ga and def2-SVP on all other atoms.^{39,40} Solvent effects were included by way of a polarizable continuum model, specifically the conductor-like polarizable continuum model, with the dielectric constant and refractive index matching DMSO.⁴¹

3. Results

We studied reactions of $\text{Ga}(\text{NO}_3)_3$ with the brominated 8-hydroquinoline ($\text{Br}_2\text{-HQH}$) in solution by UV-vis, luminescence and NMR spectroscopy, and compared the solid state properties of the $[\text{Ga}(\text{Br}_2\text{-HQ})_3]$ and the oral 8-hydroxyquinolinate anticancer complex on clinical trial $[\text{Ga}(\text{HQ})_3]$.

3.1. Reactions of $\text{Br}_2\text{-HQH}$ with $\text{Ga}(\text{NO}_3)_3$

First, we investigated the reaction between $\text{Ga}(\text{NO}_3)_3$ and 5,7-dibromo-8-hydroxyquinoline ($\text{Br}_2\text{-HQH}$) in DMSO since this solvent was found to stabilise the product. Due to solubility issues, $\text{Br}_2\text{-HQH}$ was first solubilised in DMF while the Ga(III) salt was dissolved in water. The choice of reaction media for solution studies was determined by the reasonable solubility of $\text{Br}_2\text{-HQH}$ in DMF, its poor solubility in DMSO, and insolubility in water, with our preferred use of an aqueous medium as a solvent for $\text{Ga}(\text{NO}_3)_3$ for biological relevance.

In the first titration, aqueous $\text{Ga}(\text{NO}_3)_3$ was added to $\text{Br}_2\text{-HQH}$ (0.15 mM) in 99.6% DMSO/0.4% DMF (v/v) in 0.065 mol equivalent steps to a final 1 : 1 mol ratio. As seen at Fig. 2A, $\text{Br}_2\text{-HQH}$ has absorption maxima at 330 nm and 425 nm. On addition of Ga(III) a new intense band at 390 nm appeared and continued to increase in intensity as further Ga(III) was added. There was a concomitant reduction in intensity of the $\text{Br}_2\text{-HQH}$ band at 330 nm. Notable is the isosbestic point at

355 nm, suggesting that the reaction involves an equilibrium between $\text{Br}_2\text{-HQH}$ and the $[\text{Ga}(\text{Br}_2\text{-HQ})_3]$ complex formed.

A similar titration behaviour was observed with monitoring by fluorescence ($\lambda_{\text{ex}} = 400$ nm), Fig. 2B. Initially, very weak fluorescence was observed for $\text{Br}_2\text{-HQH}$ at 530 nm, but from the addition of the first Ga(III) aliquot the band maximum red-shifted to 550 nm and increased in intensity with increasing the Ga(III) concentration, Fig. S2.‡

For less than *ca.* 7 additions of 0.065 mol equiv. Ga(III), giving a $\text{Ga}(\text{III}) : \text{Br}_2\text{-HQH}$ mol ratio $> 1 : 3$, complete formation of $[\text{Ga}(\text{Br}_2\text{-HQ})_3]$ could have occurred, but was not observed. This led us to investigate possible kinetic control of the reaction. In the next set of experiments we added either 0.33, 0.67, or 1 mol equiv. of $\text{Ga}(\text{NO}_3)_3$ to $\text{Br}_2\text{-HQH}$ (0.15 mM) in the same solvents as above (final solvent mixture 0.4% $\text{H}_2\text{O}/99.2\%$ DMSO/0.4% DMF v/v), and monitored the reaction by UV-vis every 3 min up to 300 min. In each case, a similar behaviour of decreasing intensity for the $\text{Br}_2\text{-HQH}$ band at 330 nm and increasing intensity of the 390 nm for the $[\text{Ga}(\text{Br}_2\text{-HQ})_3]$ product was observed, Fig. 3 and Fig. S3.‡ The final concentration of the product was 0.023 mM, 0.048 mM and 0.051 mM, for 0.33, 0.67, and 1 mol equiv. of $\text{Ga}(\text{NO}_3)_3$ added, respectively, *i.e.* 45, 95 and 100% formation of $[\text{Ga}(\text{Br}_2\text{-HQ})_3]$.

The absorption *versus* time plots show a reasonable fit to first order kinetics (Fig. 3, Table 1 and Fig. S3.‡) with the following rate constants: 0.15 mM Ga(III), 0.031 min⁻¹; 0.10 mM Ga(III), 0.014 min⁻¹; 0.05 mM Ga(III), 0.010 min⁻¹, suggesting that the rate-limiting step depends on the Ga(III) concentration.

The next experiment aimed to confirm the nature of the Ga(III) product, in particular the role of $\text{Br}_2\text{-HQH}$ deprotonation in the position of equilibria and in the kinetics of formation of the product. First, we generated deprotonated $\text{Br}_2\text{-HQ}$ ligand by adding NaOH solution to DMSO (0.4% DMF v/v) in steps until no further spectral changes were observed. As shown in Fig. 2C, complete deprotonation and formation of $\text{Br}_2\text{-HQ}$ was evident after addition of *ca.* 1 mol equiv. of NaOH from the decrease in intensity of the band at 330 nm and formation of two new bands at 355 nm and 425 nm for $\text{Br}_2\text{-HQ}$, accompanied by an isosbestic point at 348 nm.

Then 20 additions of $\text{Ga}(\text{NO}_3)_3$ were made to a solution of deprotonated ligand to give a final molar ratio of 1 Ga : 1 $\text{Br}_2\text{-HQ}$. In this case, the final product was fully formed in less than 0.5 mol equiv. compatible with the formation of $[\text{Ga}(\text{Br}_2\text{-HQ})_3]$ with absorption bands at 340 nm and 400 nm, Fig. 2D. To investigate the kinetics of formation of $[\text{Ga}(\text{Br}_2\text{-HQ})_3]$, 0.33 mol equiv. of Ga(III) was added to 1 mol equiv. of $\text{Br}_2\text{-HQ}$ and the reaction monitored over time. It was evident that the reaction with deprotonated ligand ($\text{Br}_2\text{-HQ}$) occurred rapidly (<3 min, Fig. S4.‡) in contrast to the reaction with the protonated ligand ($\text{Br}_2\text{-HQH}$), as described above.

3.2. Isolation and characterisation of $[\text{Ga}(\text{Br}_2\text{-HQ})_3]$

During attempts to use acetonitrile as a solvent for UV-vis titrations, we observed that a yellow precipitate readily formed when $\text{Ga}(\text{NO}_3)_3$ was added to a solution of $\text{Br}_2\text{-HQH}$. This led



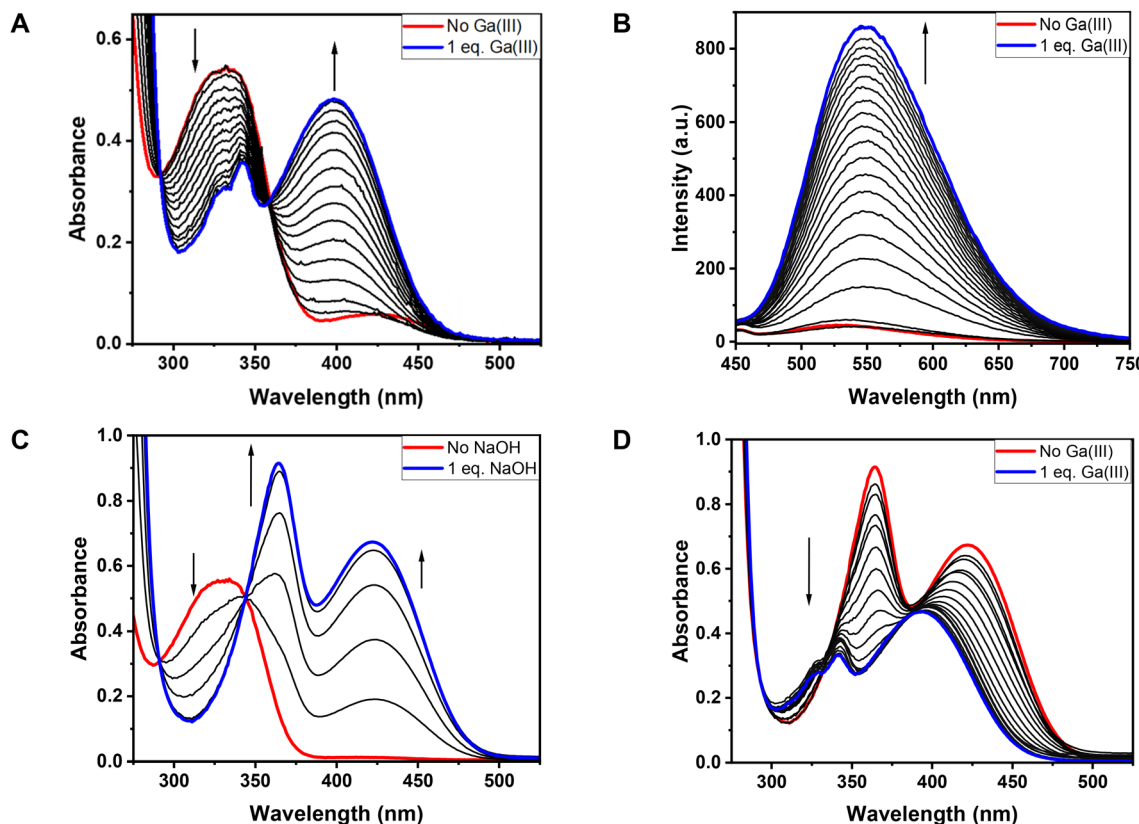


Fig. 2 (A) Changes in the UV-vis absorption spectra, and (B) emission spectra ($\lambda_{\text{ex}} = 400$ nm), when a solution of $\text{Ga}(\text{NO}_3)_3$ (0.065 mol equiv., 8 μM) in water was titrated into $\text{Br}_2\text{-HQH}$ (1 mol equiv., 0.15 mM) solution in 99.6% DMSO/0.4% DMF (v/v). (C) Changes in the UV-vis absorption spectrum when NaOH (0.2 mol equiv., 0.03 mM) was titrated into a $\text{Br}_2\text{-HQH}$ (1 mol equiv., 0.15 mM) solution in 99.6% DMSO/0.4% DMF (v/v). (D) Changes in the UV-vis absorption spectrum when a solution of $\text{Ga}(\text{NO}_3)_3$ (0.065 mol equiv., 8 μM) was titrated into deprotonated $\text{Br}_2\text{-HQ}$ (1 mol equiv., 0.15 mM) solution in 99.6% DMSO/0.4% DMF (v/v). In all the cases, the red spectrum corresponds to the initial and the blue spectrum to the final equilibrium condition.

to a convenient procedure for isolation of the $[\text{Ga}(\text{Br}_2\text{-HQ})_3]$ complex. For this, $\text{Br}_2\text{-HQH}$ was dissolved in DMF and an aqueous solution of $\text{Ga}(\text{NO}_3)_3$ were poured into acetonitrile and the yellow precipitate was isolated by filtration, washed with acetonitrile and dried, see section 2.2. The UV-vis spectrum of the complex in DMSO showed bands with maxima at 390 nm and 330 nm and a shoulder at 320 nm, Fig. S5,‡ identical to those observed during titration experiments. This product had an elemental (CHNGa) analysis, ESI-MS and IR spectra consistent with formulation as $[\text{Ga}(\text{Br}_2\text{-HQ})_3]$, Fig. S6 and S7.‡

3.3. Solution and solid-state NMR

Initially we attempted to study the binding of $\text{Br}_2\text{-HQH}$ to $\text{Ga}(\text{III})$ by solution ^1H -NMR. $\text{Ga}(\text{NO}_3)_3$ in D_2O (giving a final concentration of 4.7 mM in the NMR tube) was added to a solution of $\text{Br}_2\text{-HQH}$ in $\text{DMSO-}d_6\text{/DMF-}d_7$ (final concentration of 14 mM) and followed over time without further $\text{Ga}(\text{III})$ addition. Attempts to observe the interaction between $\text{Ga}(\text{NO}_3)_3$ and $\text{Br}_2\text{-HQH}$ by ^1H -NMR spectroscopy in the mixed solvent $\text{DMSO-}d_6\text{/DMF-}d_7\text{/D}_2\text{O}$ (58 : 32 : 10% v/v), necessary to aid solubility, gave rise to broadening of the peaks within the

aromatic region from $\text{Br}_2\text{-HQH}$ over *ca.* 1 h at 298 K, together with the appearance of low intensity peaks in the same region. Interpretation was complicated by precipitation of a product in the NMR tube.

Next, we attempted to observe the 153 MHz ^{71}Ga -NMR spectrum for a $\text{DMSO-}d_6$ solution of $[\text{Ga}(\text{Br}_2\text{-HQ})_3]$ at a concentration of 1 mM (highest concentration achievable). However, not surprisingly, in view of the quadrupolar nature of ^{71}Ga ($I = 3/2$, 39.6% abundant), the low concentration, and the expected broadening for ^{71}Ga in a non-symmetrical environment, no peak was detectable.

Next, we studied ^1H , ^{13}C and ^{71}Ga solid-state NMR spectra of $[\text{Ga}(\text{Br}_2\text{-HQ})_3]$. We hoped to take advantage of the sharpening of the multiple spin-half ^{71}Ga ($I = 3/2$) resonance at high observation frequencies.⁴² We also compared the ^{71}Ga spectra of $[\text{Ga}(\text{Br}_2\text{-HQ})_3]$ and $[\text{Ga}(\text{HQ})_3]\text{-}0.5\text{CH}_3\text{CO}_2\text{H}$ in view of the clinical use of KP46 for cancer treatment. Such spectra can provide information on the types of coordinated atoms and the coordination geometry.⁴³ No previous ^{71}Ga NMR studies of this class of bioactive complexes appear to have been reported.

Powdered samples were packed in a rotor (diameter of 1.3 mm) and ^{71}Ga solid-state spectra were recorded at 23.5 T



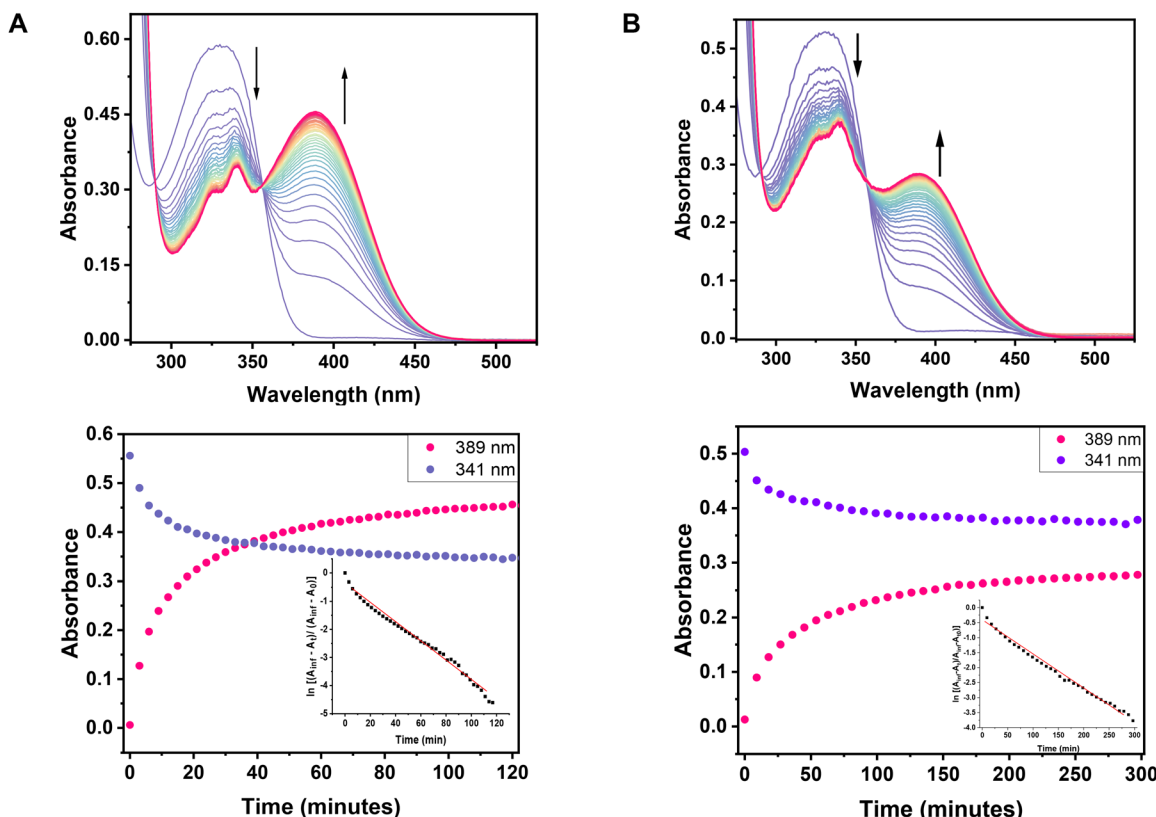


Fig. 3 (A) Top: time-dependent changes in the UV-vis absorption spectrum when $\text{Ga}(\text{NO}_3)_3$ (1 mol equiv., 0.15 mM) in water was added to $\text{Br}_2\text{-HQH}$ (1 mol equiv., 0.15 mM) solution in 99.6% DMSO/0.4% DMF (v/v). Bottom: variation in absorbance at 341 nm for $\text{Br}_2\text{-HQH}$, and 389 nm for $[\text{Ga}(\text{Br}_2\text{-HQ})_3]$ with time. (B) Top: time-dependent changes in the UV-vis absorption spectrum when $\text{Ga}(\text{NO}_3)_3$ (0.33 mol equiv., 0.05 mM) in water was added to $\text{Br}_2\text{-HQH}$ (1 mol equiv., 0.15 mM) solution in 99.6% DMSO/0.4% DMF (v/v). Bottom: variation in absorbance at 341 nm for $\text{Br}_2\text{-HQH}$, and 389 nm for $[\text{Ga}(\text{Br}_2\text{-HQ})_3]$ with time. The insets show the best fit of $\log A$ vs. time (red line), giving the first-order rate constants in Table 1.

Table 1 Rates of reaction of Ga(III) with $\text{Br}_2\text{-HQH}$ in 0.4% H_2O /99.2% DMSO/0.4% DMF v/v, 298 K at various mol ratios

Mol ratio (Ga : $\text{Br}_2\text{-HQH}$)	[Ga] (mM)	Observed rate ^a (min^{-1})
1 : 1	0.15	0.031
0.67 : 1	0.10	0.014
0.33 : 1	0.05	0.010

^a Determined by UV-vis assuming first order kinetics, Fig. 3 and Fig. S2.‡

⁷¹Ga Lamor frequency of 305 MHz) with 60 kHz MAS for $[\text{Ga}(\text{Br}_2\text{-HQ})_3]$ and $[\text{Ga}(\text{HQ})_3]$, Fig. 4. As expected, at 20 T (260 MHz ⁷¹Ga) the resonances were slightly broader (Fig. 4). Fitting the signals to one Ga site for each complex indicated similar isotropic chemical shifts of $\delta^{(71)\text{Ga}} = 101$ and 98 ppm, for $[\text{Ga}(\text{Br}_2\text{-HQ})_3]$ and $[\text{Ga}(\text{HQ})_3]\text{0.5CH}_3\text{CO}_2\text{H}$, respectively. Analysis of line shapes at 20 and 23.5 T gave rise to a quadrupolar coupling constant of $C_Q = 9 \pm 0.5$ MHz with a quadrupolar asymmetry parameter of $\eta = 0.5 \pm 0.15$ for both complexes $[\text{Ga}(\text{Br}_2\text{-HQ})_3]$ and $[\text{Ga}(\text{HQ})_3]\text{0.5CH}_3\text{CO}_2\text{H}$.

The 1 GHz ¹H-DPMAS-NMR spectrum for $[\text{Ga}(\text{HQ})_3]\text{0.5CH}_3\text{CO}_2\text{H}$ showed a distinct pattern of resonances which

can be divided into two regions, 4 to 6 ppm attributable to the phenolic region of the complex, and 6 to 10 ppm assignable to pyridyl ring protons, Fig. 5A. The additional peak at -0.8 ppm can be assigned to the methyl group of acetic acid. Aqueous acetic acid was used as solvent in the synthesis, see section 2.3. The presence of acetic acid was also evident from the solution ¹H-NMR spectrum, a singlet for the acetic acid methyl protons at 1.8 ppm and another at 11.9 ppm assignable to the carboxylic acid proton, integrating as 0.5 mol acetic acid per mol of $[\text{Ga}(\text{HQ})_3]$, Fig. S1.‡

For $[\text{Ga}(\text{Br}_2\text{-HQ})_3]$, the presence of the two bromide substituents on the hydroquinolinate ligands gives rise to a shift of the phenolic ring protons to low field compared to $[\text{Ga}(\text{HQ})_3]$, but the resonances for individual protons are unresolved, Fig. 5A.

¹H-¹H NOESY solid-state NMR spectra were recorded with mixing times of 5 ms and 220 ms, Fig. 6 and Fig. S8.‡ For $[\text{Ga}(\text{HQ})_3]\text{0.5CH}_3\text{CO}_2\text{H}$ with a 5 ms mixing time, two cross peaks for ¹H signals at -0.8/5 ppm and -0.8/8 ppm are evident, and indicative of close contact between the acetic acid and hydroxyquinolinate ring protons, as well as less well-resolved cross-peaks between the ring protons. These cross-peaks became broader with a mixing time of 220 ms. For $[\text{Ga}(\text{Br}_2\text{-HQ})_3]$ the

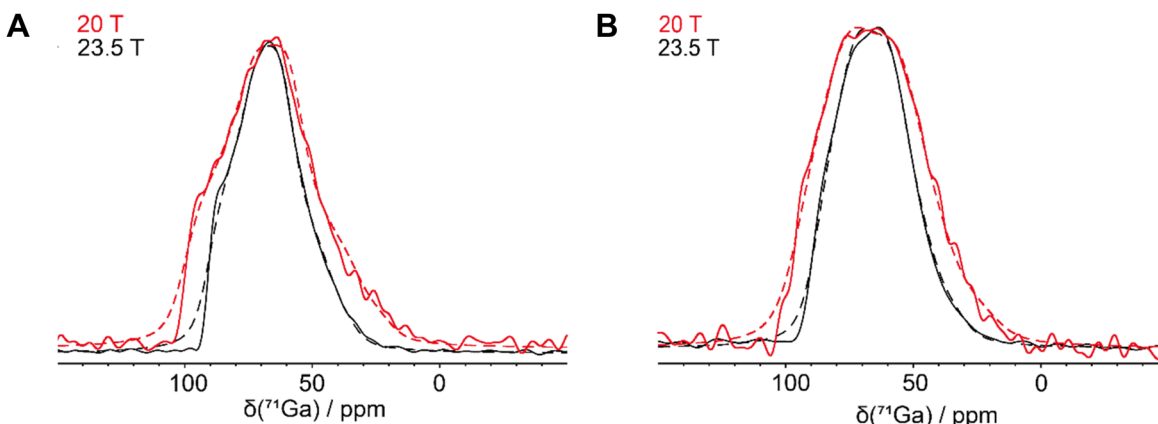


Fig. 4 ^{71}Ga solid state MAS NMR spin-echo spectra recorded at 259 MHz (red) or 306 MHz (black) (A) $[\text{Ga}(\text{Br}_2\text{-HQ})_3]$, and (B) $[\text{Ga}(\text{HQ})_3]\text{-}0.5\text{CH}_3\text{CO}_2\text{H}$. The peaks were fitted as single sites (red dashed and black dashed lines). Spectra are scaled to equal maxima. The narrowing of peaks at higher frequency is evident.

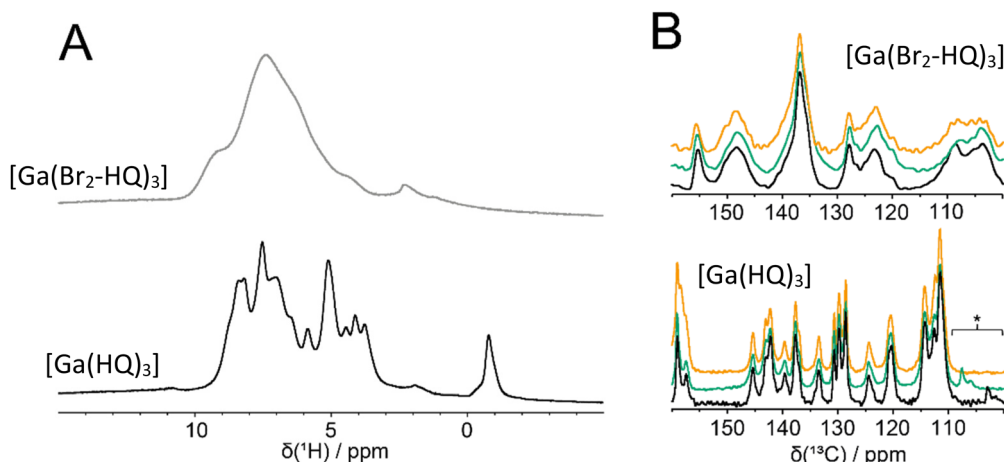


Fig. 5 (A) ^1H NMR solid-state NMR spectra of $[\text{Ga}(\text{Br}_2\text{-HQ})_3]$ and $[\text{Ga}(\text{HQ})_3]\text{-}0.5\text{CH}_3\text{CO}_2\text{H}$ recorded at 23.5 T (1 GHz). (B) 20 T (214 MHz) ^{13}C solid state CPMAS NMR spectra of $[\text{Ga}(\text{Br}_2\text{-HQ})_3]$ (top) and $[\text{Ga}(\text{HQ})_3]\text{-}0.5\text{CH}_3\text{CO}_2\text{H}$ (bottom) at spinning rates of 10 kHz (black), 11 kHz (blue) and 12 kHz (orange). Peaks assigned to the complexes have chemical shifts independent of spinning rate. * = Spinning side bands.

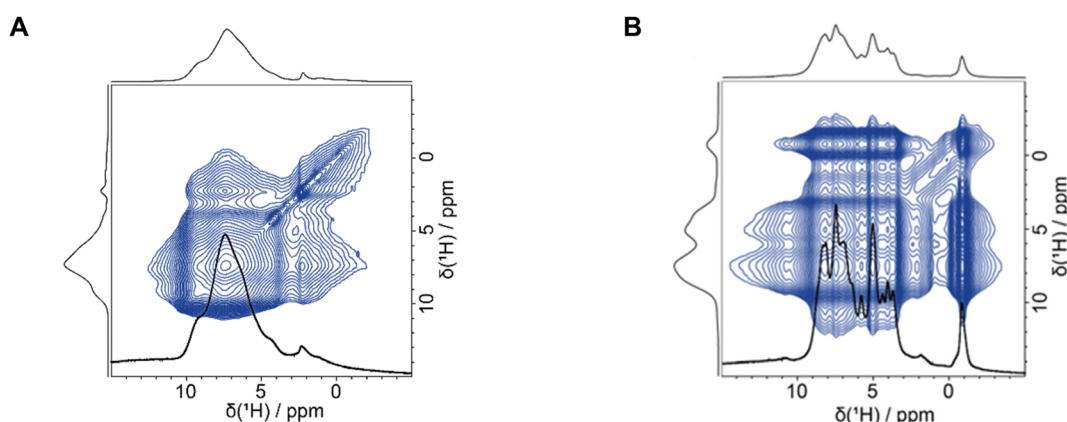


Fig. 6 ^1H - ^1H NOESY solid state MAS spectra at 850 MHz of (A) $[\text{Ga}(\text{Br}_2\text{-HQ})_3]$ and (B) $[\text{Ga}(\text{HQ})_3]\text{-}0.5\text{CH}_3\text{CO}_2\text{H}$ (mixing time of 220 ms).



NOESY cross peaks were poorly resolved with a 5 ms mixing time, but better resolved at 220 ms for contacts between HQ protons.

The ^{13}C CPMAS spectrum of $[\text{Ga}(\text{HQ})_3] \cdot 0.5 \text{CH}_3\text{CO}_2\text{H}$ (Fig. 5B) also showed sharper peaks than for $[\text{Ga}(\text{Br}_2\text{-HQ})_3]$, as for ^1H -NMR spectra. The ^{13}C CPMAS spectra of the protonated free ligands HQH and $\text{Br}_2\text{-HQH}$ also showed sharp peaks, Fig. S9,‡ indicating crystalline properties. The resonances of HQH and $\text{Br}_2\text{-HQH}$ were assigned on the basis of reported solution spectra.^{44,45} Both, ^{13}C and ^1H resonances for $[\text{Ga}(\text{Br}_2\text{-HQ})_3]$ are broadened compared to $[\text{Ga}(\text{HQ})_3] \cdot 0.5\text{CH}_3\text{CO}_2\text{H}$. The broadened resonances for $[\text{Ga}(\text{Br}_2\text{-HQ})_3]$ indicate disorder in the sample, whereas the ^{13}C CPMAS spectrum of $[\text{Ga}(\text{HQ})_3] \cdot 0.5 \text{CH}_3\text{CO}_2\text{H}$ has more than nine resolved peaks showing its high crystallinity and the non-equivalence of the coordinated ligands.

3.4. Photophysical characterisation

As shown in Fig. 2B, $[\text{Ga}(\text{Br}_2\text{-HQ})_3]$ in DMSO has an emission at 550 nm. Upon pulsed laser excitation at 405 nm, a short lifetime of 1.32 ns was observed suggesting that it is fluorescence originating from a singlet excited state (S_1), Fig. S10.‡ $[\text{Ga}(\text{Br}_2\text{-HQ})_3]$ appeared to be poorly photostable since continuous irradiation at 420 nm led to a 13% decrease in intensity of the band at 400 nm in 15 min without the appearance of new bands, Fig. S11.‡

Several DFT functionals (see section 2.11) were employed to calculate UV-Vis absorption spectra, Fig. S12.‡ The best agreement with experiment was obtained using the B3LYP functional with DFT-D3 dispersion correction,^{46,47} however the character of the S_1 transition differed from those predicted by every other method used. Therefore, we calculated vacuum excited state energies with the high-accuracy wave function-based method ADC(2) and arrived at the best theoretical estimate for both absorption and emission by using the ADC(2) $S_0 \rightarrow S_1$ excitation in vacuum and adding the respective hypsochromic and bathochromic shift for solvent and relaxation effects from $\omega\text{B97X-D3}$ ⁴⁸ calculations, Table S1.‡ This resulted in wavelengths of 390 nm for the absorption of the S_1 state and a fluorescence at 539 nm out of the same state. These values compare well with the experimentally measured wavelengths of 405 and 550 nm. Therefore, both absorption and emission originate from the S_1 state. The T_1 state was found at excitation wavelengths longer than 500 nm and phosphorescence above 700 nm for all functionals, therefore it was discounted as the source of luminescence.

Calculations on $[\text{Ga}(\text{HQ})_3]$ showed qualitatively similar absorption behaviour to $[\text{Ga}(\text{Br}_2\text{-HQ})_3]$, with the former exhibiting a slight hypsochromic shift with respect to the Br-substituted molecule, Fig. S13.‡ Additionally, the calculations provided insight into the preferred geometry of $[\text{Ga}(\text{Br}_2\text{-HQ})_3]$ for which the meridional isomer is slightly more stable than the facial isomer, in both vacuum and DMSO conditions, Table S2.‡

4. Discussion

There is much interest in the design of Ga(III) complexes as anticancer and antimicrobial agents, and in particular tris-hydroxyquinolinate complexes, one of which, $[\text{Ga}(\text{HQ})_3]$, is undergoing preclinical trials as an anticancer agent.⁴⁹ We studied reactions between dibromo-hydroxyquinoline and increasing concentrations of Ga(III) in DMSO/H₂O at mol ratios of ligand : Ga(III) of 1 : 0.33, 1 : 0.67, 1 : 1. Previous reports using potentiometry have shown the high stability of $[\text{Ga}(\text{HQ})_3]$ and sulfonated derivative in water,^{50,51} as well as step-wise formation of the sulfonated complex.⁵¹ In general, tris-chelated complexes $[\text{Ga}(\text{X-HQ})_3]$ are more thermodynamically stable compared to the mono- and bis-chelated species.⁵² However, such equilibria in aqueous media are complicated by the hydrolytic chemistry of Ga(III) in aqueous media which involves a range of monomeric and polymeric hydroxido/oxido species.^{21,53} Analogous species have been widely studied for Al(III),^{54,55} Fe(III),^{56,57} and In(III).^{58,59} Here, we have studied the formation of Ga(III) complexes with the brominated hydroxyquinoline ligand $\text{Br}_2\text{-HQH}$ (Fig. 1) with a view to mapping reactions of the tris-chelate $[\text{Ga}(\text{Br}_2\text{-HQ})_3]$ in intact cells using X-ray fluorescence. Detection of both Ga(III) and bromine would allow monitoring of possible ligand displacement, as we have shown recently with organo-osmium anticancer agents.²⁴ Such studies may be valuable for identifying the active components (pharmacophores) in cells.

First, we studied the step-wise addition of $\text{Br}_2\text{-HQH}$ to Ga(III) monitored by UV-vis and fluorescence spectroscopy, Fig. 2A and B. These reactions were studied in a variety of mixed aqueous solvents compatible with the solubility of $\text{Ga}(\text{NO}_3)_3$ and $\text{Br}_2\text{-HQH}$. $[\text{Ga}(\text{Br}_2\text{-HQ})_3]$ formed readily in the presence excess Ga(III), however complete formation of the product required a large excess of Ga(III) in the mixed solvent 99.2% DMSO/0.4% DMF/0.4% H₂O (v/v). In contrast, titration of deprotonated ligand with Ga(III) led to stoichiometric formation of $[\text{Ga}(\text{Br}_2\text{-HQ})_3]$, Fig. 2C and D. This difference can be explained by the presence of basic Ga-hydroxido species in the titration of $\text{Br}_2\text{-HQH}$ which deprotonate the ligand.

The formation of such Ga(III)-hydroxido monomers and polymers has been studied previously.^{21-23,60} At nanomolar Ga concentrations, mainly monomeric species are formed in aqueous solution with Ga(OH)^{2+} predominating at pH 3 to 4 with further deprotonation leading to Ga(OH)_4^- predominating at pH $> ca. 4.2$.⁶⁰ At millimolar concentrations, oligomeric species such as $\text{Ga}_4(\text{OH})_{11}^+$ predominate at pH *ca.* 4 and $\text{Ga}(\text{OH})_3$ at pH 7 and $\text{Ga}(\text{OH})_4^-$ at pH 8.²¹ Hence, we assume that in our mixed aqueous solvent such hydroxido species will readily form and act as bases to deprotonate the $\text{Br}_2\text{-HQH}$ ligand. The possibility that DMSO and NO_3^- can also be involved in mixed aqua/ligand complexes and affect the pK_a values of bound water cannot be ruled out.^{61,62} No attempt was made to determine the pH values in our mixed solvents.

UV-vis studies showed that the reaction of $\text{Ga}(\text{NO}_3)_3$ with $\text{Br}_2\text{-HQH}$ is relatively slow taking >2 h to reach completion, Fig. 3 and Fig. S3.‡ For such reactions, a single isosbestic



point was observed at 355 nm suggesting an overall conversion of $\text{Br}_2\text{-HQH}$ into a single product.

At the different molar ratios of $\text{Ga} : \text{Br}_2\text{-HQH}$, the kinetic plots gave a reasonable 1st-order fit with half-lives of 22.4 min, 49.5 min, 69.1 min, with $\text{Ga}(\text{m})$ concentration increasing from 0.33 equiv. to 1 equiv., respectively, showing an approximate linear dependence on $\text{Ga}(\text{m})$ concentration (Fig. 3, Fig. S3‡ and Table 1). At equilibrium the overall yield of $[\text{Ga}(\text{Br}_2\text{-HQ})_3]$ relative to the initial concentration of $\text{Br}_2\text{-HQH}$ was *ca.* 100%, 85% and 45% mol equiv. with 1, 0.67 and 0.33 mol equiv. of $\text{Ga}(\text{m})$, respectively.

Further detailed kinetic studies of these reactions are warranted, but were beyond the scope of the present work. The reaction mechanism for formation of $[\text{Ga}(\text{Br}_2\text{-HQ})_3]$ is complicated and likely to involve sequential binding of three $\text{Br}_2\text{-HQH}$ to $\text{Ga}(\text{m})$, perhaps *via* initial coordination of hydroxyquinoline N to $\text{Ga}(\text{m})$, followed by chelate ring formation *via* deprotonation of the hydroxyl group. The formation of the second and third chelate rings is further complicated by the possible formation of isomers (*cis/trans* and *fac/mer*). Since the reaction of deprotonated $\text{Br}_2\text{-HQH}$ with $\text{Ga}(\text{m})$ proceeded rapidly (*ca.* 3 min, Fig. S4‡), it seems likely that the rate-limiting step is ring closure *via* -OH deprotonation. Basic hydroxido $\text{Ga}(\text{m})$ species seem likely to be involved in this step.

There appear to be few reports of kinetics and mechanisms of ligand substitution reactions for $\text{Ga}(\text{m})$. Such studies are potentially important for understanding the (dynamic) metalomics of bioactive $\text{Ga}(\text{m})$ complexes in biological media.

Initial attempts to isolate $[\text{Ga}(\text{Br}_2\text{-HQ})_3]$ using protocols reported in the literature^{63,64} were unsuccessful, until we discovered that the product readily precipitated in acetonitrile. By dissolving $\text{Br}_2\text{-HQH}$ in DMF followed by addition of acetonitrile and then $\text{Ga}(\text{NO}_3)_3$ in a minimum volume of water, a yellow precipitate readily formed. This protocol is similar to that described for chelation of 5,7-dihalo-8-quinolinolone to $\text{Sn}(\text{IV})$ ⁶⁴ (*i.e.*, with no base addition).

In the UV-vis spectrum in DMSO, the band at 400 nm is assignable to ligand–ligand charge transfer (LLCT) as confirmed by DFT calculations, Fig. S12.‡ As is normally the case for $\text{nd}^{10}(n+1)\text{s}^0$ metals, no ligand-to-metal (LMCT) band was seen for $[\text{Ga}(\text{Br}_2\text{-HQ})_3]$, as reported for isostructural $[\text{Al}(\text{HQ})_3]$.^{65,66}

Additional characterisation of $[\text{Ga}(\text{Br}_2\text{-HQ})_3]$ was obtained from the Fourier-transform infrared (FT-IR) spectrum, Fig. S6.‡ The comparison between the free ligand and complex clearly showed the disappearance of the broad -OH peak of hydroxyquinoline (at $\sim 3000 \text{ cm}^{-1}$) and the appearance of two new peaks at 950 and 1110 cm^{-1} assignable to $\text{Ga}(\text{m})\text{-O}$ bonds, analogous to $\text{Al}(\text{m})$ and $\text{In}(\text{m})$ complexes.⁶⁷

The low solubility of $[\text{Ga}(\text{Br}_2\text{-HQ})_3]$ made characterisation by NMR in solution difficult. We therefore recorded ^{71}Ga -, ^1H - and ^{13}C solid-state NMR spectra for $[\text{Ga}(\text{Br}_2\text{-HQ})_3]$ and compared to $[\text{Ga}(\text{HQ})_3]$ which was synthesized as $[\text{Ga}(\text{HQ})_3]\cdot 0.5\text{CH}_3\text{CO}_2\text{H}$. As seen in Fig. 4, the two complexes have a similar ^{71}Ga chemical shift (101 and 98 ppm, for $[\text{Ga}(\text{Br}_2\text{-HQ})_3]$ and $[\text{Ga}(\text{HQ})_3]\cdot 0.5\text{CH}_3\text{CO}_2\text{H}$, respectively). These chemi-

cal shifts are in the range that might be expected for hexacoordinated $\text{Ga}(\text{m})$ complexes.⁶⁸ Both complexes in this study had a coordination sphere of 3N and 3O. In a similar environment, but with six-coordinated NOTA-type ligands bound to $\text{Ga}(\text{m})$, reported ^{71}Ga chemical shifts are in the range +110 to +171 ppm.⁶⁹ Thus the chemical shifts observed here are within the expected region for 3N and 3O hexacoordinated $\text{Ga}(\text{m})$ complexes. This appears to be the first report of ^{71}Ga data for $\text{Ga}(\text{m})$ coordinated to hydroxyquinolate ligands. The reported range of ^{71}Ga shifts is *ca.* +700 to -700 ppm ,^{70–73} however there are too few to enable a more detailed correlation of chemical shifts with number and/or types of coordinated ligand and the coordination geometry.

It is notable that the ^{71}Ga quadrupole coupling constant observed here ($C_Q = 9 \pm 0.5 \text{ MHz}$) is higher compared to Ga bound to carboxylate groups⁷⁴ and lower compared to Ga bound to siloxides⁷⁵ suggesting that the resonance signature is closely dependent on the local symmetry of gallium.⁷⁶ In the case of $[\text{Ga}(\text{Br}_2\text{-HQ})_3]$ and $[\text{Ga}(\text{HQ})_3]$ the local symmetry is also affected by the different isomers (*facial* vs. *meridional*), in the solid and liquid states. $\text{Ga}(\text{m})$ preferably adopts the less symmetric but more energetically stable *mer*-configuration.⁷⁷ This correlates with the ^{13}C CPMAS and ^1H DPMAS data and DFT calculations.

^1H - ^1H NOESY spectra for $[\text{Ga}(\text{HQ})_3]\cdot\text{CH}_3\text{CO}_2\text{H}$ (Fig. 6 and Fig. S8‡) indicate spatial proximity of protons in the complexes, including the interaction of quinolinate protons (5 to 10 ppm), with acetic acid methyl protons at $\sim 0.8 \text{ ppm}$. The role of such small molecules in the solid-state structure of this anticancer drug might be important for its formulation for drug use, influencing its rate of dissolution and absorption, and is worthy of further investigation.

In the ^{13}C CPMAS and ^1H DPMAS solid-state NMR spectra for both complexes there was an increase in the number of hydroxyquinoline peaks compared to those of the free ligand, Fig. 5 and Fig. S9.‡ From this observation, it can be deduced that these $\text{Ga}(\text{m})$ complexes are likely to be to *meridional* isomers rather than the more symmetrical *facial* isomers, as in the reported X-ray crystal structure of $[\text{Ga}(\text{HQ})_3]$.^{78,79}

Fluorescence of $[\text{Ga}(\text{Br}_2\text{-HQ})_3]$ was observed at 550 nm ($\lambda_{\text{ex}} = 400 \text{ nm}$) in DMSO solution (Fig. 1). Interestingly, *mer*- $[\text{Al}(\text{HQ})_3]$ emits at 525 nm whereas the *fac* isomer emits at the shorter wavelength of 475 nm.⁸⁰ Excited state calculations based on energetics, suggested the emission is likely to arise from the S_1 state, similar to the experimental findings here, as the triplet T_1 state is too low in energy, Table S1.‡

Double hybrid and range-separated functionals predict the S_1 state to be a localized, ligand-centred (LC), transition on one ligand (Fig. 7). Whilst B3LYP provides the best agreement with respect to experiment, it shows vastly different character for the S_1 state than the other XC functionals, instead predicting S_1 to be of ligand–ligand CT (44%) and LC character. A comparison of absorption spectra of $[\text{Ga}(\text{Br}_2\text{-HQ})_3]$ *in vacuo* and in DMSO showed that the solvent causes a blue-shift by *ca.* 0.2 eV for all tested functionals. In summary, the best theoretical estimate shows that emission in DMSO originates



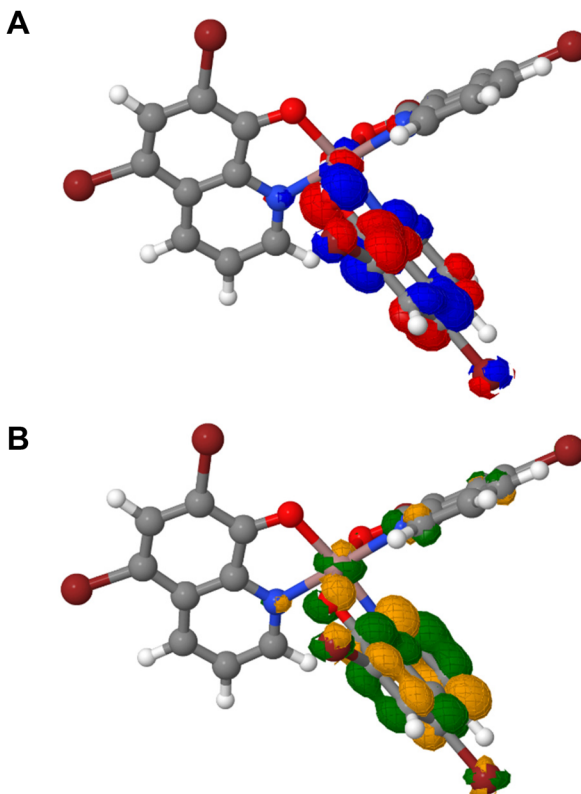


Fig. 7 Natural transition orbitals for the $S_0 \rightarrow S_1$ excitation of $[\text{Ga}(\text{Br}_2\text{-HQ})_3]$, obtained using the TD- ω B97X-D3 functional in DMSO. The structures show (A) the electron density before, and (B) immediately after excitation. Both are localised mostly on a ligand; indicative of a ligand-centred (LC) transition.

from the S_1 state at 539 nm which is a reasonable fit to the experimental emission at 550 nm. DFT calculations showed that *mer*- $[\text{Ga}(\text{Br}_2\text{-HQ})_3]$ is slightly more thermodynamically stable compared to the *fac* isomer in both DMSO (by *ca.* 5 to 7 kJ mol^{-1}) and vacuum (by *ca.* 26 to 30 kJ mol^{-1}), Table S2.[‡]

5. Conclusions

There is much current interest in the anticancer and antimicrobial activity of $\text{Ga}(\text{III})$ complexes.^{81,82} In this work we have obtained new insights into the chemistry of $\text{Ga}(\text{III})$ tris-hydroxy-quinolinate complexes, particularly focusing on the synthesis, stability, and structure of the novel $[\text{Ga}(\text{Br}_2\text{-HQ})_3]$ complex. By employing UV-vis, fluorescence, NMR spectroscopy and DFT calculations, the work provides a detailed comparison of $[\text{Ga}(\text{Br}_2\text{-HQ})_3]$ with the clinically relevant $[\text{Ga}(\text{HQ})_3]$. The findings suggest that basic $\text{Ga}(\text{III})$ hydroxido species can play a crucial role in hydroxyquinoline ligand deprotonation on formation of these complexes. The comparison between $[\text{Ga}(\text{Br}_2\text{-HQ})_3]$ and the clinical tris-8-hydroxyquinolinate complex $[\text{Ga}(\text{HQ})_3]$ using high-field solid state revealed second coordination sphere interactions between an acetic acid solvent molecule and the bound hydroxyquinolinate ligands in $[\text{Ga}(\text{HQ})_3]\cdot 0.5\text{CH}_3\text{CO}_2\text{H}$.

The discovery of such interactions suggests that carboxylic acids and related molecules might facilitate the design of new formulations of the drug to control release rates in anticancer and antimicrobial applications. The presence of both Ga and Br as elements readily detectable by *e.g.* XRF and ICP-MS, provides a possible strategy for investigate chelated ligand release from $\text{Ga}(\text{III})$ in intact biological cells, as well as delivery by vehicles such as SiO_2 nanoparticles.

Author contributions

RCM and PJS designed the project. VVG synthesised $[\text{Ga}(\text{Br}_2\text{-HQ})_3]$ and performed the IR, in-solution NMR, UV-vis and fluorescence experiments with analysis assisted by PJS and RCM. RCM synthesised $[\text{Ga}(\text{HQ})_3]$. SB and DI conceptualized and performed high-field NMR experiments, with contributions from RCM. LC, AWP and MJP performed the DFT calculations. All authors contributed to the writing and editing of the drafts, led by RCM.

Data availability

The data supporting this article have been included as part of the ESI.[‡]

Conflicts of interest

There are no conflicts to declare.

Acknowledgements

This work was supported by the European Union's Horizon 2020 research and innovation programme under the Marie Skłodowska-Curie grant agreement No. 945380 (for RCM), EPSRC (grant no. EP/F034210/1 and EP/P030572/1), and the UK High-Field Solid-State NMR National Research Facility (project no. 240742). M. J. P. acknowledges EPSRC for funding through Grant No. EP/T021675 and EP/V006746. A. W. P and M. J. P. acknowledge the Leverhulme Trust (grant No. RPG-2020-208). We also thank the Warwick Centre for Ultrafast Spectroscopy for use of the Horiba Fluorolog, and Dr Russell Needham for assistance with ICP, Ms Joanna Drozd with MS, and Dr Ivan Prokes with solution state NMR.

References

- 1 W. Sun, M. Qi, S. Cheng, C. Li, B. Dong and L. Wang, *Mater. Des.*, 2023, 227, 111704.
- 2 C. R. Chitambar, *Future Med. Chem.*, 2012, 4, 1257–1272.
- 3 J. E. Blower, M. S. Cooper, C. Imberti, M. T. Ma, C. Marshall, J. D. Young and P. J. Blower, *Radiopharm. Chem.*, 2019, 255, 271.



4 J. P. Lavender, J. Lowe, J. R. Barker, J. I. Burn and M. A. Chaudhri, *Br. J. Radiol.*, 1971, **44**, 361–366.

5 C. R. Chitambar, *Expert Opin. Investig. Drugs*, 2004, **13**, 531–541.

6 P. J. Blower, R. Cusnir, A. Darwesh, N. J. Long, M. T. Ma, B. E. Osborne, T. W. Price, J. Pellico, G. Reid, R. Southworth, G. J. Stasiuk, S. Y. A. Terry and R. T. M. de Rosales, *Adv. Inorg. Chem.*, 2021, **78**, 1–35.

7 C. R. Chitambar, *Future Med. Chem.*, 2012, **4**, 1257–1272.

8 C. R. Chitambar, *Biochim. Biophys. Acta, Mol. Cell Res.*, 2016, **1863**, 2044–2053.

9 A. Frei, J. Zuegg, A. G. Elliott, M. Baker, S. Braese, C. Brown, F. Chen, C. G. Dowson, G. Dujardin, N. Jung, A. P. King, A. M. Mansour, M. Massi, J. Moat, H. A. Mohamed, A. K. Renfrew, P. J. Rutledge, P. J. Sadler, M. H. Todd, C. E. Willans, J. J. Wilson, M. A. Cooper and M. A. T. Blaskovich, *Chem. Sci.*, 2020, **11**, 2627–2639.

10 A. Frei, A. G. Elliott, A. Kan, H. Dinh, S. Bräse, A. E. Bruce, M. R. Bruce, F. Chen, D. Humaidy, N. Jung, A. P. King, P. G. Lye, H. K. Maliszewska, A. M. Mansour, D. Matiadis, M. P. Muñoz, T.-Y. Pai, S. Pokhrel, P. J. Sadler, M. Sagnou, M. Taylor, J. J. Wilson, D. Woods, J. Zuegg, W. Meyer, A. K. Cain, M. A. Cooper and M. A. T. Blaskovich, *JACS Au*, 2022, **2**, 2277–2294.

11 M. G. Best, C. Cunha-Reis, A. Y. Ganin, A. Sousa, J. Johnston, A. L. Oliveira, D. G. E. Smith, H. H. P. Yiu and I. R. Cooper, *ACS Appl. Bio Mater.*, 2020, **3**, 7589–7597.

12 X. X. Peng, H. Zhang, R. Zhang, Z. H. Li, Z. S. Yang, J. Zhang, S. Gao and J. L. Zhang, *Angew. Chem., Int. Ed.*, 2023, **62**, e202307838.

13 K. B. Patel and P. Kumari, *J. Mol. Struct.*, 2022, **1268**, 133634.

14 M. Ilakiyalakshmi and A. A. Napoleon, *Arabian J. Chem.*, 2022, **15**, 104168.

15 A. M. F. Darwesh, C. Imberti, J. J. Bartnicka, F. Al-Saleemee, J. E. Blower, A. Rigby, J. Bordoloi, A. Griffiths, M. T. Ma and P. J. Blower, *Molecules*, 2023, **28**, 7217.

16 R. M. Cornell, R. Giovanoli and W. Schneider, *J. Chem. Technol. Biotechnol.*, 1989, **46**, 115–134.

17 B. Batchelor, J. B. McEwen and R. Perry, *Environ. Sci. Technol.*, 1986, **20**, 891–889.

18 S. Bi, C. Wang, Q. Cao and C. Zhang, *Coord. Chem. Rev.*, 2004, **248**, 441–455.

19 C. Wang, T. Yang, Y. Liu, J. Ruan, S. Yang and X. Liu, *Int. J. Hydrogen Energy*, 2014, **39**, 10843–10852.

20 J. M. Bigham and D. K. Nordstrom, *Rev. Mineral. Geochem.*, 2000, **40**, 351–403.

21 B. Hacht, *Bull. Korean Chem. Soc.*, 2008, **29**, 372–376.

22 Y. Toporivska, A. Mular, K. Piasta, M. Ostrowska, D. Illuminati, A. Baldi, V. Albanese, S. Pacifico, I. O. Fritsky, M. Remelli, R. Guerrini and E. Gumienna-Kontecka, *Inorg. Chem.*, 2021, **60**, 13332–13347.

23 H. V. T. Luong and J. C. Liu, *Sep. Purif. Technol.*, 2014, **132**, 115–119.

24 E. M. Bolitho, J. P. C. Coverdale, H. E. Bridgewater, G. J. Clarkson, P. D. Quinn, C. Sanchez-Cano and P. J. Sadler, *Angew. Chem., Int. Ed.*, 2021, **60**, 6462–6472.

25 J. Ren and H. Eckert, *J. Phys. Chem. C*, 2014, **118**, 15386–15403.

26 P. Collery, J. L. Domingo and B. K. Keppler, *Anticancer Res.*, 1996, **16**, 687–692.

27 C. R. Morcombe and K. W. Zilm, *J. Magn. Reson.*, 2003, **162**, 479–486.

28 B. Elena, G. de Paëpe and L. Emsley, *Chem. Phys. Lett.*, 2004, **398**, 532–538.

29 M. Goswami, P. J. M. Van Bentum and A. P. M. Kentgens, *J. Magn. Reson.*, 2012, **219**, 25–32.

30 Ē. Kupce and R. Freeman, *J. Magn. Reson., Ser. A*, 1995, **117**, 246–256.

31 U. Ekström, L. Visscher, R. Bast, A. J. Thorvaldsen and K. Ruud, *J. Chem. Theory Comput.*, 2010, **6**, 1971–1980.

32 F. Neese, *Wiley Interdiscip. Rev.: Comput. Mol. Sci.*, 2022, **12**, e1606.

33 F. Neese, *Wiley Interdiscip. Rev.: Comput. Mol. Sci.*, 2022, **2**, 73–78.

34 D. Mester and M. Kállay, *J. Chem. Theory Comput.*, 2019, **15**, 4440–4453.

35 D. Mester, P. R. Nagy and M. Kállay, *J. Chem. Phys.*, 2018, **148**, 094111.

36 D. Mester, P. R. Nagy and M. Kállay, *J. Chem. Theory Comput.*, 2019, **15**, 6111–6126.

37 M. Kállay, P. R. Nagy, D. Mester, Z. Rolik, G. Samu, J. Csontos, J. Csóka, P. B. Szabó, L. Gyevi-Nagy, B. Hégely, I. Ladjánszki, L. Szegedy, B. Ladóczki, K. Petrov, M. Farkas, P. D. Mezei and Á. Ganyecz, *J. Chem. Phys.*, 2020, **152**, 074107.

38 Mrcc, a quantum chemical program suite written by M. Kállay, P. R. Nagy, D. Mester, L. Gyevi-Nagy, J. Csóka, P. B. Szabó, Z. Rolik, G. Samu, J. Csontos, B. Hégely, Á. Ganyecz, I. Ladjánszki, L. Szegedy, B. Ladóczki, K. Petrov, M. Farkas, P. D. Mezei and R. A. Horváth, see <https://www.mrcc.hu>, <https://www.mrcc.hu/index.php/citation>, (accessed 23 October 2024).

39 F. Weigend and R. Ahlrichs, *Phys. Chem. Chem. Phys.*, 2005, **7**, 3297–3305.

40 A. Schäfer, H. Horn and R. Ahlrichs, *J. Chem. Phys.*, 1992, **97**, 2571–2577.

41 J. Tomasi and M. Persico, *Chem. Rev.*, 1994, **94**, 2027–2094.

42 K. Chen, *Int. J. Mol. Sci.*, 2020, **21**, 1–22.

43 B. Reif, S. E. Ashbrook, L. Emsley and M. Hong, *Nat. Rev. Methods Primers*, 2021, **1**, 2.

44 J. Kidrič, D. Hadži, D. Kocjan and V. Rutar, *Org. Magn. Reson.*, 1981, **15**, 280–284.

45 S. Ökten, O. Çakmak, A. Saddiq, B. Keskin, S. Özdemir and M. Inal, *Org. Commun.*, 2016, **9**, 82–93.

46 A. D. Becke, *J. Chem. Phys.*, 1993, **98**, 5648–5652.

47 S. Grimme, J. Antony, S. Ehrlich and H. Krieg, *J. Chem. Phys.*, 2010, **132**, 154104.

48 Y. S. Lin, G. De Li, S. P. Mao and J. Da Chai, *J. Chem. Theory Comput.*, 2013, **9**, 263–272.

49 N. L. Wilke, L. O. Abodo, C. Frias, J. Frias, J. Baas, M. A. Jakupc, B. K. Keppler and A. Prokop, *Biomed. Pharmacother.*, 2022, **156**, 113974.



50 É.A Enyedy, O. Dömöötör, E. Varga, T. Kiss, R. Trondl, C. G. Hartinger and B. K. Keppler, *J. Inorg. Biochem.*, 2012, **117**, 189–197.

51 P. Letkeman, A. E. Martell and R. J. Motekaitis, *J. Coord. Chem.*, 1980, **10**, 47–53.

52 M. Thompson, *Anal. Chim. Acta*, 1978, **98**, 357–363.

53 W. Yuan, J. Chen, H. Teng, B. Chetelat, H. Cai, J. Liu, Z. Wang, J. Bouchez, F. Moynier, J. Gaillardet, J. Schott and C. Liu, *Global Biogeochem. Cycles*, 2021, **35**, e2021GB007033.

54 E. Lydersen, *Nord. Hydrol.*, 1990, **21**, 195–204.

55 W. R. Harris, G. Berthon, J. P. Day, C. Exley, T. P. Flaten, W. F. Forbes, T. Kiss, C. Orvig and P. F. Zatta, *J. Toxicol. Environ. Health, Part A*, 1996, **48**, 543–568.

56 A. Stefánsson, *Environ. Sci. Technol.*, 2007, **41**, 6117–6123.

57 R. H. Byrne, Y. R. Luo and R. W. Young, *Mar. Chem.*, 2000, **70**, 23–35.

58 D. Ferri, *Acta Chem. Scand.*, 1972, **26**, 747–759.

59 S. A. Wood and I. M. Samson, *Ore Geol. Rev.*, 2006, **28**, 57–102.

60 K. Hagvall, P. Persson and T. Karlsson, *Geochim. Cosmochim. Acta*, 2014, **146**, 76–89.

61 A. Molla-Abbassi, M. Skripkin, M. Kritikos, I. Persson, J. Mink and M. Sandström, *Dalton Trans.*, 2003, **9**, 1746–1753.

62 W. W. Rudolph and C. C. Pye, *Phys. Chem. Chem. Phys.*, 2002, **4**, 4319–4327.

63 X. Zhou, *J. Inorg. Biochem.*, 2023, **238**, 112051.

64 O. T. Alexander, M. M. Duvenhage, A. Brink, H. C. Swart, P. Müller, R. E. Kroon and H. G. Visser, *J. Coord. Chem.*, 2017, **70**, 1316–1326.

65 A. Curioni, M. Boero and W. Andreoni, *Chem. Phys. Lett.*, 1998, **294**, 263–271.

66 M. Brinkmann, B. Fite, S. Pratontep and C. Chaumont, *Chem. Mater.*, 2004, **16**, 4627–4633.

67 C. F. R. A. C. Lima, R. J. S. Taveira, J. C. S. Costa, A. M. Fernandes, A. Melo, A. M. S. Silva and L. M. N. B. F. Santos, *Phys. Chem. Chem. Phys.*, 2016, **18**, 16555–16565.

68 C. O. Areán, M. R. Delgado, V. Montouillout and D. Massiot, *Z. Anorg. Allg. Chem.*, 2005, **631**, 2121–2126.

69 J. P. André and H. R. Mäcke, *J. Inorg. Biochem.*, 2003, **97**, 315–323.

70 S. M. Bradley, R. F. Howe and J. V. Hanna, *Solid State Nucl. Magn. Reson.*, 1993, **2**, 37–46.

71 S. M. Bradley, R. F. Howe and R. A. Kydd, *Magn. Reson. Chem.*, 1993, **31**, 883–886.

72 (Ga) Gallium NMR, <https://chem.ch.huji.ac.il/nmr/techniques/1d/row4/ga.html>, (last accessed 10 January 2025).

73 L. Ronconi and P. J. Sadler, *Coord. Chem. Rev.*, 2008, **252**, 2239–2277.

74 C. Volkringer, T. Loiseau, G. Férey, C. M. Morais, F. Taulelle, V. Montouillout and D. Massiot, *Microporous Mesoporous Mater.*, 2007, **105**, 111–117.

75 S. R. Docherty, L. A. Völker, A. V. Yakimov, R. Verel and C. Copéret, *J. Phys. Chem. C*, 2023, **127**, 24552–24563.

76 P. Becker, T. Wonglakhon, D. Zahn, D. Gudat and R. Niewa, *Chem. – Eur. J.*, 2020, **26**, 7008–7017.

77 M. L. Ramos, A. R. E. De Sousa, L. L. G. Justino, S. M. Fonseca, C. F. G. C. Geraldes and H. D. Burrows, *Dalton Trans.*, 2013, **42**, 3682–3694.

78 Y. Wang, W. Zhang, Y. Li, L. Ye and G. Yang, *Chem. Mater.*, 1999, **11**, 530–532.

79 M. Rajeswaran and V. V. Jarikov, *Acta Crystallogr., Sect. E: Struct. Rep. Online*, 2004, **60**, m217–m218.

80 M. Goswami, P. K. Nayak, N. Periasamy and P. K. Madhu, *Chem. Cent. J.*, 2009, **3**, 1–11.

81 L. M. O'Ferrall, A. Fantasia, K. Chan, L. M. Teixeira, K. Kavanagh, C. O'Connor, M. A. Santos, S. Chaves, V. M. Nurchi, G. Crispioni, M. A. Zoroddu, D. M. Griffith and R. Cappai, *J. Inorg. Biochem.*, 2024, **259**, 112663.

82 X. X. Peng, S. Gao and J. L. Zhang, *Eur. J. Inorg. Chem.*, 2022, e202100953.

